Journal of Power Sources 195 (2010) 4758–4764

Contents lists available at ScienceDirect

Journal of Power Sources

journal homepage: www.elsevier.com/locate/jpowsour

# Alternative perovskite materials as a cathode component for intermediate temperature single-chamber solid oxide fuel cell

Cyril Gaudillère[a], Louis Olivier[a], Philippe Vernoux[a], Chunming Zhang[b], Zongping Shao[b], David Farrusseng[a,*]

[a] Université Lyon 1, CNRS, UMR 5256, IRCELYON, Institut de recherches sur la catalyse et l'environnement de Lyon, 2 avenue Albert Einstein, F-69626 Villeurbanne, France
[b] State Key Laboratory of Materials-Oriented Chemical Engineering, College of Chemistry & Chemical Engineering, Nanjing University of Technology, No 5 Xin Mofan Road, Nanjing 210009, PR China

ARTICLE INFO

*Article history:*
Received 24 November 2009
Received in revised form 1 February 2010
Accepted 21 February 2010
Available online 26 February 2010

*Keywords:*
Single-chamber solid oxide fuel cell
Cathode
Perovskite materials
Intermediate temperature
Hydrocarbon

ABSTRACT

This paper exploits the suitability of three perovskite materials $Ba_{0.5}Sr_{0.5}Co_{0.8}Fe_{0.2}O_{3-\delta}$ (BSCF), $GdBaCo_2O_{5+\delta}$ (GBC) and $Ba_{0.5}Sr_{0.5}Mn_{0.7}Fe_{0.3}O_{3-\delta}$ (BSMF) as SOFC cathodes in the single-chamber configuration operating at the intermediate temperature range. TG analysis showed high thermal stability depending on the crystalline phases of the materials. The catalytic activity of these three materials for hydrocarbon conversion was investigated under a realistic feed, i.e. with hydrocarbon, oxygen, water and carbon dioxide. Electrochemical impedance spectroscopy of the various cathodes tested in symmetric cell configuration revealed a B-site dependence of the electrode catalytic activity for oxygen reduction. High temperature (1000 °C) powder reactivity tests over a gadolinium doped-ceria (CGO) and perovskite cathode revealed excellent chemical compatibility of BSMF and CGO. Catalytic tests associated with thermal and structural characterization attest to the suitability of these materials in the single-chamber configuration.



## 1. Introduction

Solid oxide fuel cells (SOFCs) are considered as promising systems for efficient (>50% yield), environmental friendly (no $NO_x$), and reliable electrical energy production. Currently, conventional SOFC systems, which operate at typically around 1000 °C, are based on a Ni-YSZ (8 mol% $Y_2O_3$ doped $ZrO_2$) cermet as an anode compound, a LSM (lanthanum Strontium Manganite $LaSrMnO_3$) perovskite as a cathode, and are fed with a mixture of $H_2$ (as a fuel source) and air (as an oxidant). Such a system has been demonstrated on an industrial scale. However, this type of configuration has numerous limitations to overcome before it can enter the market. Namely, these obstacles include difficulties in $H_2$ distribution and storage as well as high operating temperature necessary to a high electrolyte ionic conductivity and limited cell ohmic resistance. An innovative configuration called single-chamber SOFC (SC-SOFC) [1–3] recently demonstrated the ability to overcome the above concerns. The main difference to conventional dual-chamber SOFC is that a mixture of hydrocarbon fuel and air is supplied over both electrodes. Such a cell configuration exhibits several advantages suggesting less complexity in commercialization including quicker start up, simpler cell design leading to the minimization of problem due to the gas control, and sealing [4]. Even if significant efforts decrease working temperature of SOFC down to the intermediate range of 600 °C, the implementation of the conventional electrode material in commercial process is unlikely. Indeed, common electrodes induce a loss of power density in the single-chamber SOFC concept, due to a drop of electromotive force (EMF) between the two electrodes caused mainly by a finite hydrocarbon conversion on the cathode and high electrode polarization resistances because of the poor electrochemical activity of the electrodes. Therefore, both electrode materials shall be adapted and optimized to selectively allow catalytic reactions and high electrochemical performances. Since the driving force for the ionic conduction through the electrolyte is the difference of oxygen thermodynamic activities at both electrodes, the catalytic challenge at the cathode is the electrochemical reduction of oxygen coupled with a high electronic conductivity, while avoiding hydrocarbon activation and conversion [5]. In addition, the chemical compatibility between new cathode materials needs and the components must be investigated to ensure long-term reliability of the system. The high temperature required during the fabrication process may result in potential reactivity between the different layers as previously described [6,7], leading to the formation of an insulating phase detrimental to the electrical and ionic conductivities.

* Corresponding author.
*E-mail address:* david.farrusseng@ircelyon.univ-lyon1.fr (D. Farrusseng).

0378-7753/$ – see front matter © 2010 Elsevier B.V. All rights reserved.
doi:10.1016/j.jpowsour.2010.02.058

Among the various potential cathode materials, perovskites are widely investigated due to their high electronic conductivity, good activity for the electrochemical oxygen reduction associated with high ionic conductivity, and favourable stability at elevated temperatures. Due to the flexibility of the crystallographic structure of the perovskite, an infinite combination of composition is theoretically possible by substitution. By tailoring the cation, the electronic and ionic conductivities can be optimized. Generally the substitution of B sites by cobalt cations improves the ionic conductivity of the perovskite [8].

The perovskite $Ba_{0.5}Sr_{0.5}Co_{0.8}Fe_{0.2}O_{3-\delta}$, denoted as BSCF, and widely studied in the last few years, is a very interesting reference cathode material in the intermediate temperature range due its relatively high electronic conductivity and low catalytic activity towards hydrocarbon conversion [9,10]. Shao et al. [4] have used this material as a cathode material at 650 °C under methane atmosphere and demonstrated a very interesting peak of power density of 760 mW $cm^2$. Nevertheless, this material presents some drawbacks like the possible diffusion of cations like $Sm^{3+}$ containing Sm-doped-ceria electrolyte inside the perovskite structure [11,12]. Moreover, the exposure of BSCF to hydrocarbons could lead to $CO_2$ production, that would induce the formation of carbonates at temperatures as low as 300 °C [13] and thus the degradation of the cathode. Our objective is the development of new cathode materials for single-chamber SOFCs. Herein, we report synthesis, thermal and electrical characterizations, and the catalytic performances under realistic feed conditions of $Ba_{0.5}Sr_{0.5}Mn_{0.7}Fe_{0.3}O_{3-\delta}$ (BSMF), $Ba_{0.5}Sr_{0.5}Co_{0.8}Fe_{0.2}O_{3-\delta}$ (BSCF) and $GdBaCo_2O_{5+\delta}$ (GBC) as potential cathode candidates for a single-chamber SOFC configuration.

## 2. Experimental

### 2.1. Material preparation

The perovskite compositions investigated in this paper include BSCF as a reference material, BSMF as an innovative phase, and the brownmillerite structure GBC which has been deeply characterized by Tarancón et al. [7–14]. Samples were synthesized by the nitrate-citrate method [15]. Metal nitrates (purchased from Sigma–Aldrich, purity > 99%) were dissolved in water with the required proportion of citric acid and EDTA (purchased from Sigma–Aldrich). After 2 h under vigorous stirring, the final solution was heated until 100 °C to evaporate water then dried in an oven at 120 °C for 2 h. The resulting powders were heated in air at a rate of 2 °C $min^{-1}$ and maintained for 4 h at 900, 1200 and 1040 °C for BSCF, BSMF and GBC, respectively.

### 2.2. Material characterization

Elementary analysis was carried out by Inductively Coupled Plasma ICP (Activa Horiba) after samples were dissolved. Structure was investigated by powder X-ray diffraction (PXRD) using a Bruker D5005 Diffractometer with the Cu Kα radiation at λ = 0.15418 nm. Thermogravimetric (TG) and differential thermal (DT) measurements were recorded with a thermal analyzer (Setaram, Setsys Evolution 12, crucible PtRh 10%) over the three samples in the temperature range 25–750 °C under air (50 mL $min^{-1}$) with a ramp of 2 °C $min^{-1}$.

The specific surface areas were determined by $N_2$ physisorption at 77 K by the BET measurement method (ASAP 2020 Micromeritics) after desorption under $10^{-2}$ mbar at 300 °C for 6 h. Porous structural data are summarized in Table 1.

Catalytic tests were carried out in a Switch 16 parallel reactor (AMTEC GmbH-CNRS). The detail information about the reactor has been described elsewhere [16]. Reactors were filled with 100 mg of catalysts and submitted to a so-called "single-chamber" feed consisted of a 2% hydrocarbon concentration (methane or propane) diluted in air (20% $O_2$ + Ar) with a total flow of 50 mL $min^{-1}$. The O/C ratio is fixed at 20. Then, addition of 20% of water and 5% of carbon dioxide to the former "single-chamber" feed was performed to simulate SOFC real working conditions. The corresponding O/C ratios are 30 with addition of water and 35 with 5% $CO_2$ additional. The temperature range investigated for these catalytic tests was 400–600 °C and each analysis was duplicated after 12 and 22 min under flow to detect catalyst deactivation. Exhaust gases were analyzed by a gas chromatography (GC HP 6950 and 6980) allowing quantification of $H_2$, CO, $CO_2$, $CH_4$ and $C_3H_8$. Water potentially produced during reaction was condensed in a Peltier cooler placed before the GC analysis.

Electrochemical impedance spectroscopy was conducted based on a symmetric cell using a two-electrode arrangement. The BSMF and GBC slurries were painted onto both surfaces of a CGO pellet (calcined at 1500 °C with a diameter of 10 mm) in a symmetric configuration and subsequently calcinated for 2 h under an air atmosphere at 1100 and 1000 °C for BSMF and GBC, respectively. Data were collected in the temperature range (450–750 °C) using an electrochemical workstation composed of a Solartron 1260A frequency response analyzer and a Solartron 1287 potentiostat under an air atmosphere. The applied frequency range was from 0.01 Hz to 100 kHz, and the signal amplitude was 10 mV under open-circuit voltage (OCV) conditions. Silver paste was used as the current collector over both cathode sides. All results presented here correspond to one cathode and are normalized with the electrode area.

Study of powder reactivity was performed by mixing synthesized powered samples with $Ce_{0.9}G_{0.1}O_{1.95}$ (CGO 10% with $S_{BET}$ = 12.4 $m^2$ $g^{-1}$ provided by Rhodia) in the weight ratio of 50:50. The mixture was intimately grinded in an agate mortar and then annealed at the following high temperatures 800, 900 or 1000 °C in air for 50 h. CGO has been chosen as an electrolyte due to its very interesting ionic conductivity around 600 °C. YSZ displayed poor performance in the suggested temperature range due to its low ionic conductivity [17]. Then, any experiment with YSZ has been performed.

## 3. Results

### 3.1. Textural and composition features

Specific surface areas for the three perovskite materials are summarized in Table 1. The values are low with the largest surface area found for GBC with a value of 2.8 $m^2$ $g^{-1}$. This observation is in accordance with our previous studies where perovskite materials often exhibit low values of specific surface area due to their high temperature of calcination. Table 1 also gives the theoretical and experimental molar fractions of elements in each sample. Experimental values are quite close to the theoretical values testifying to the synthesis authenticity. The Ba content for the GBC sample displayed the largest deviation between the theoretical values. This discrepancy can be explained by the volatilization of the cation dur-

**Table 1**
Specific surface areas measured by $N_2$ physisorption and theoretical/experimental molar fractions (%) of each element measured by Inductively Coupled Plasma (ICP) analysis.

| | $S_{BET}$ ($m^2$ $g^{-1}$) | Ba | Sr | Co | Fe | Mn | Gd |
|---|---|---|---|---|---|---|---|
| BSCF | 1.8 | 25/24 | 25/24.3 | 40/41.5 | 10/10.2 | / | / |
| BSMF | 2.2 | 25/24.4 | 25/25.8 | / | 15/14.9 | 35/34.9 | / |
| GBC | 2.8 | 25/20.3 | / | 50/53.1 | / | / | 25/26.5 |

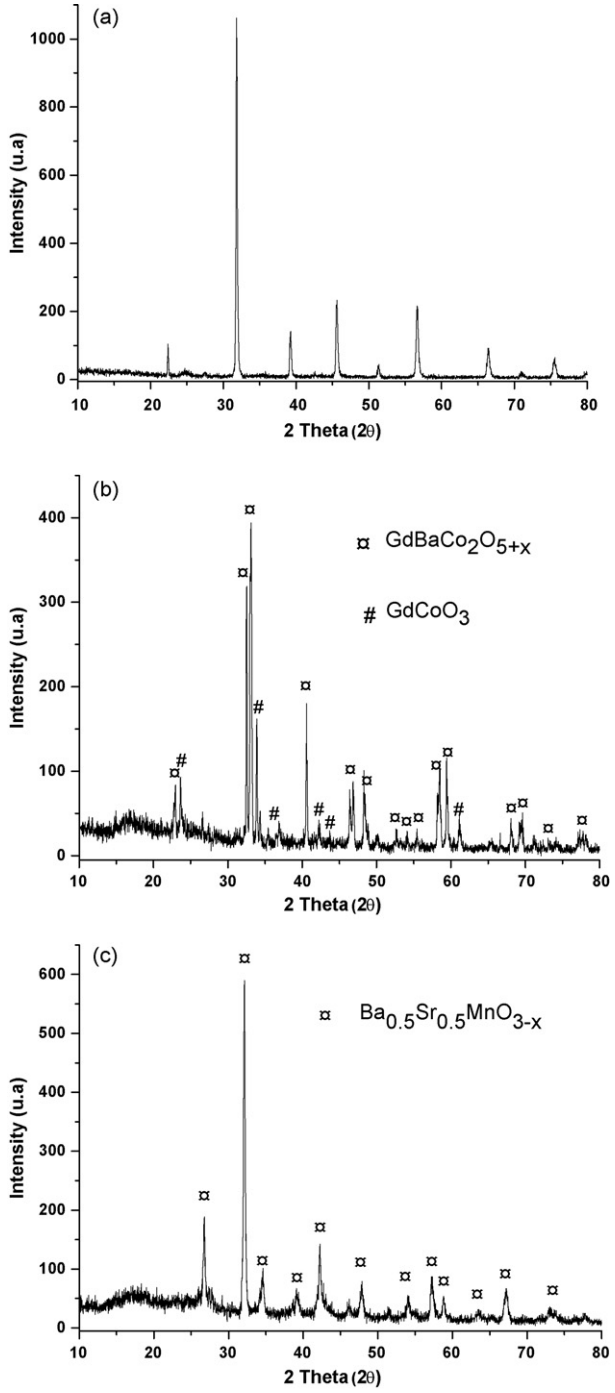


**Fig. 1.** (a) XRD patterns for $Ba_{0.5}Sr_{0.5}Co_{0.8}Fe_{0.2}O_{3-\delta}$. (b) XRD pattern for $GdBaCo_2O_{5+\delta}$. XRD pattern for $Ba_{0.5}Sr_{0.5}Mn_{0.7}Fe_{0.3}O_{3-\delta}$.

ing the calcination step and the higher energy necessary for the Ba cation to be inserted in the lattice.

### 3.2. XRD characterization

Fig. 1a–c give the X-ray diffraction patterns for the three synthesized samples. BSCF can be indexed in the cubic system with the *Pm*3*m* space group, and agrees well with previous studies by Wei et al. [10] (Fig. 1a). GBC pattern (Fig. 1b) exhibits two phases corresponding to the GBC system which crystallized in the orthorhombic system with the *Pmmm* space group and a parasitic phase indexed as $GdCoO_3$. This observation corroborates the

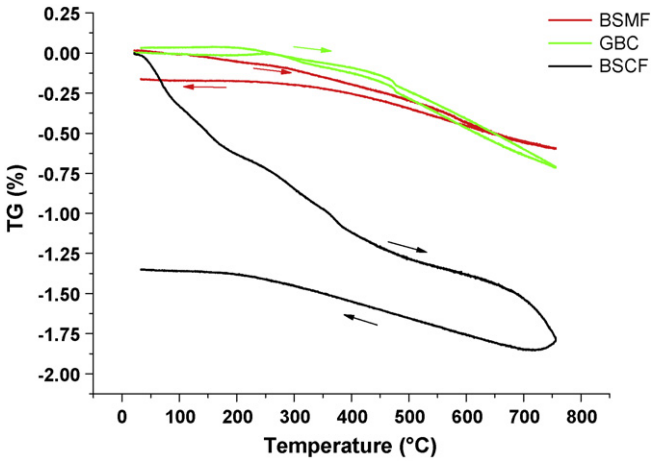


**Fig. 2.** Thermogravimetric measurements over BSMF, BSCF and GBC under air.

marked gap between experimental and theoretical Ba molar fraction (Table 1). The volatilization of Ba leads to the formation of a secondary phase. This phase is also crystallized in the orthorhombic system but with the *Pnma* space group. A higher crystallization level, and the disappearing of the parasitic phase, could be achieved with a longer time of calcination. Indeed, in previous work, the authors have found that several calcination cycles were necessary to obtain highly pure crystalline compound [14]. Despite this additional phase, this powder was chosen for the following experiments.

Concerning the BSMF compound, no data is available for the material in the JCPDS files. Thus, the indexation was done based on the undoped material $Ba_{0.5}Sr_{0.5}MnO_{3-\delta}$. This material crystallizes in the hexagonal system with the *P*63/*mmc* space group. Our powder BSMF was well indexed with the corresponding JCPD file as seen in Fig. 1c. This observation suggests that the insertion of 30 mol% of iron in the structure does not generate phase transition or evolution of lattice parameter probably due to the match between both Mn and Fe cations ($Mn^{3+/4+}$ = 0.72/0.67 Å and $Fe^{3+/4+}$ = 0.78/0.72 Å).

### 3.3. TG/DT analysis

To ascertain the stability of our materials in the intermediate temperature range, thermogravimetric and differential thermal measurements were performed under air at a maximum temperature of 750 °C.

Thermogravimetric measurements, as a function of temperature during the heating and cooling steps, are presented in Fig. 2 for BSMF and GBC.

The BSCF sample showed a total weight loss of about 1.75% at 750 °C, comparable with previous results [10]. During the heating step, BSMF and GBC samples lost weight. These samples exhibit a limited weight loss with a maximum of 0.7% for GBC and 0.6% for BSMF at 750 °C, much less than BSCF. Nevertheless, for the three samples, the total amount of desorbed species can be considered low. The global weight loss can be mainly attributed to the desorption of water for the low temperatures (<150 °C) and the release of oxygen molecules from the lattice due to slight equilibrium shifts at higher temperatures. The cooling step pointed out two distinct behaviours. The weight loss is reversible for GBC compared to BSMF and BSCF samples where only 0.45% and 0.5% of the initial weight is recovered, respectively.

As it can be seen in the Fig. 3, GBC is the only sample presenting structural modifications. Indeed, two structural changes are outstanding at 76 °C and 476 °C. During the heating ramp, the phenomenon is endothermic while, during the cooling step, it is exothermic.

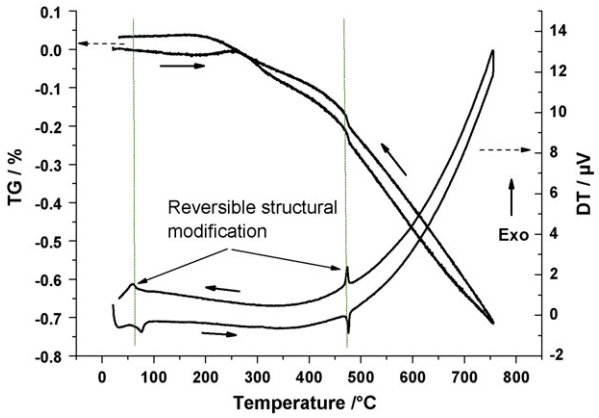


**Fig. 3.** Thermogravimetric (TG) and differential thermal (DT) measurements over GBC under air. Arrows indicate the heating and cooling steps.

Such observations were already reported in the literature [14–18] indicating no modification of the thermal expansion coefficient (TEC) value despite the phase transition from an orthorhombic to a tetragonal system. Furthermore, the accurate matching of temperature structural modifications for the samples demonstrated that the main phase, $GdBaCo_2O_{5+x}$, is predominant in the synthesized powder.

### 3.4. Catalytic screening

The three perovskite samples were catalytically tested towards hydrocarbon conversion to determine the suitable ones for the cathode in a single-chamber SOFC. Samples were first submitted to a flow containing 2% of hydrocarbon in air followed by heating to a temperature between 400 °C and 600 °C. A blank analysis showed that no conversion was observed even at high temperatures after discarding the gas phase contribution. Fig. 4 reports the methane (**a**) and propane (**b**) conversions over the samples under the present conditions.

Catalytic tests were first performed over LSM (30% wt Sr and $S_{BET} = 26.1\ m^2\ g^{-1}$), the conventional cathode material, in order to establish a benchmark for a material as a single-chamber SOFC component [19] in the intermediate temperature range. Indeed, the methane conversion over this material was already about 15% at 400 °C, the upper limit that may be considered to avoid a drop of EMF in the SC-SOFC system. At 600 °C, we observed a full conversion of hydrocarbon. The three perovskites GBC, BSCF and BSMF presented interesting results with low conversion over the temperature range investigated. From 550 °C, the methane conversion for BSMF increases. At 600 °C, it reaches 30%. Regardless of the sample, no syngas was generated, and the only product detected by gas chromatography was $CO_2$ with a selectivity of 1. Thus, we concluded that only hydrocarbon combustion reaction occurs over these samples.

Propane conversion, as a function of temperature, is presented in Fig. 4(b). No test was performed over LSM material because of its high methane conversion. As previously seen under methane atmosphere, BSMF presents a different behaviour compared with the other samples with a marked increase of propane conversion at 550 °C. At 600 °C, about 90% of conversion is reached. BSCF and GBC follow the same tendency, i.e. a gradual increase of conversion with temperature, with less than 10% at 400 °C to 35% at 600 °C. Here again, only hydrocarbon combustion is promoted.

In order to simulate real SOFC working conditions, samples were submitted to a flow containing methane, oxygen, water and carbon dioxide with a ratio 2:20:20:5 with argon as balance at a temperature range of 400 °C and 600 °C. Fig. 5 depicts the methane conversion as a function of temperature.

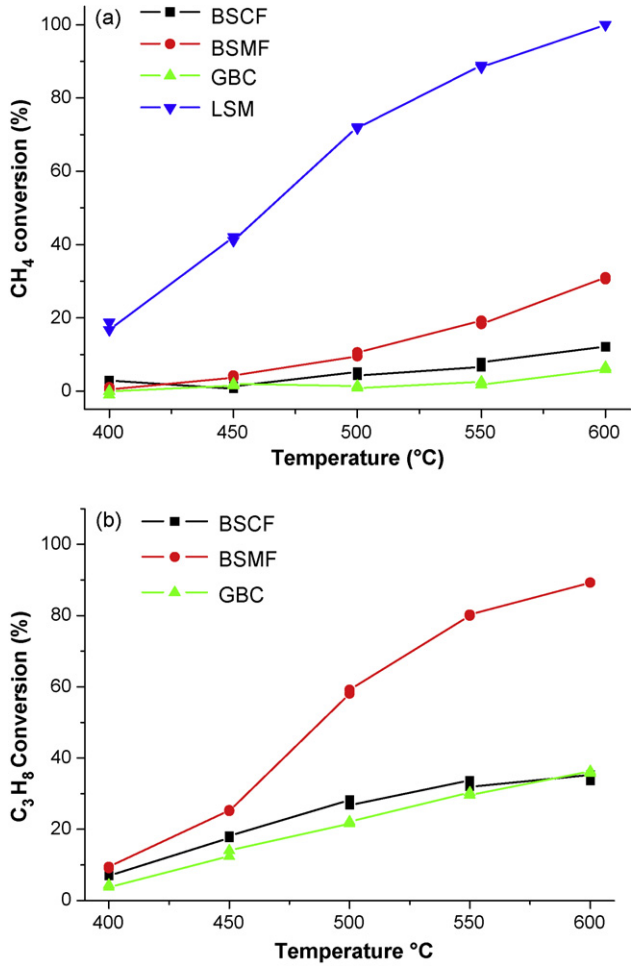


**Fig. 4.** $CH_4$ and $C_3H_8$ conversion as a function of temperature under 2% $CH_4$ (a) and 2% $C_3H_8$ (b) in air. The total flow is 50 mL min$^{-1}$.

In the presence of water and carbon dioxide at low temperatures, LSM perovskite is less active for methane conversion when compared to the same reaction under dry methane (25% of conversion against 70% previously at 500 °C). Nevertheless, the full

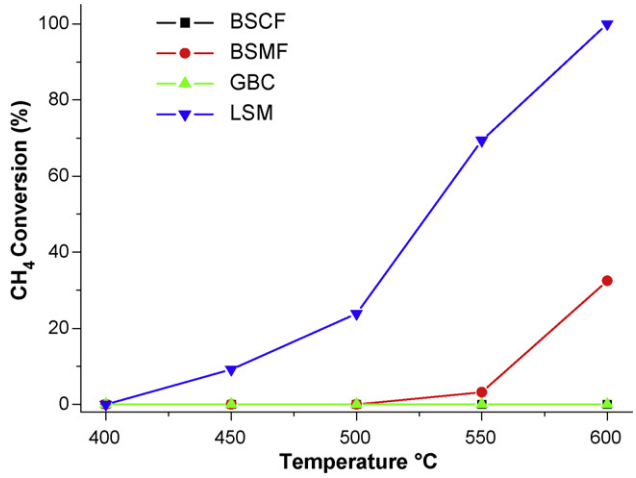


**Fig. 5.** $CH_4$ conversion as a function of temperature under methane, oxygen, water and carbon dioxide with the ratio (2:20: 20: 5) and Ar as balance. The total flow is 50 mL min$^{-1}$.

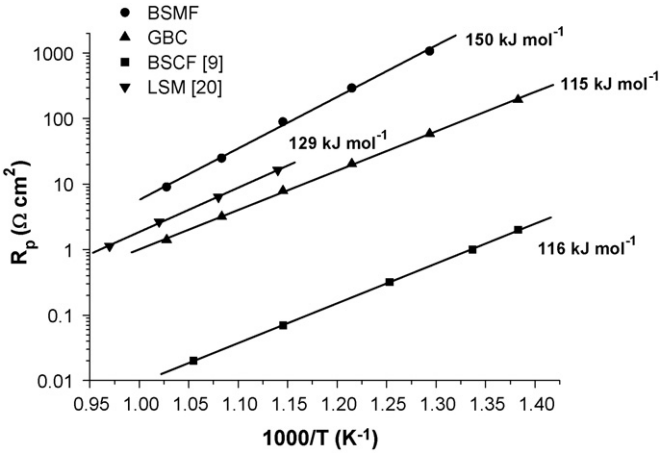


**Fig. 6.** Temperature dependence of ASRs of BSCF, BSMF and GBC cathodes measured on CGO in air.

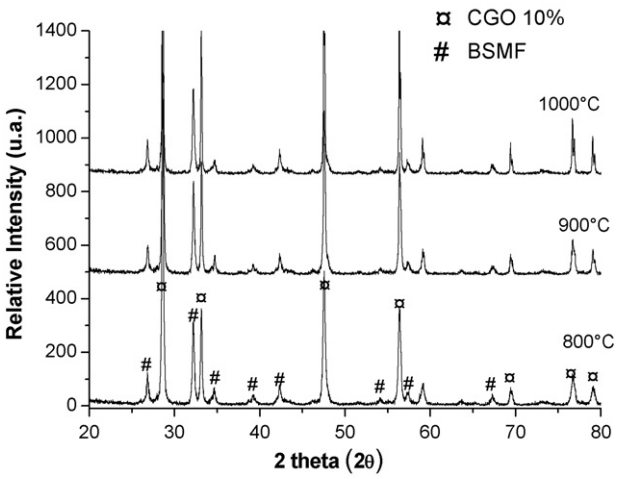


**Fig. 7.** XRD patterns for the 50:50 weight mix of BSMF and CGO powders after 50 h at 800 °C, 900 °C and 1000 °C under air.

conversion is reached at 600 °C. Unfortunately, values are still too high, which do not satisfy the maximum conversion limit. BSCF and GBC are fully inactive for the methane conversion over the entire temperature range considered. Here again, BSMF exhibited a different trend with methane combustion beginning at temperature in the upper 500 °C and reaching a maximum of about 28% at 600 °C. No syngas was produced, only water was recovered in the Peltier cooler and $CO_2$ was analyzed.

These experiments demonstrated that these materials meet the targeted catalytic requirements for a SOFC cathode in the single-chamber configuration.

### 3.5. Electrode performance

Fig. 6 presents the area specific resistances (ASRs) of the electrodes in Arrhenius plots, measured over symmetrical cells with CGO as an electrolyte and BSMF and GBC cathodes under air. Typical ASR values corresponding to BSCF and LSM deposited over CGO were gathered from the literature as a reference [9–20]. For all tested samples, the plots were linear at reciprocal temperatures with variable slopes pointing out the difference of activity towards oxygen electrochemical reduction. The activation energy for oxygen reduction is about 115 kJ $mol^{-1}$ over GBC; similar with BSCF values from the literature [8]. Nevertheless, the values of cathodic ASR are significantly higher for the GBC material compared to the BSCF material with values of 7.5 Ω $cm^2$ and 0.07 Ω $cm^2$, respectively. On the other hand, values for GBC are still lower than LSM values under the same conditions. BSMF/CGO symmetrical cell presents a higher energy of activation than LSM for oxygen reduction with the value about 150 kJ $mol^{-1}$ and thus higher ASRs values. As an example, the area specific resistance reached 80 Ω $cm^2$ at 600 °C. GBC and BSCF are thus promising candidates as a substitute for LSM with a focus on the electrical properties.

### 3.6. Chemical reactivity

Among cathode requirements, the reactivity with the electrolyte is the primary concern for practical applications and has to be taken in account to avoid assembly leading to the formation of additional phases as previously described [6]. To overcome this situation, studies have pointed out the interest of an interlayer between the electrolyte and the cathode, for example CGO between YSZ and BSCF [21]. Nevertheless, the polarization resistance, attributed to accumulation of layers in the SOFC stack has to be decreased to avoid power loss. The main solutions to achieve this goal are to decrease the layers thickness or find a cathode/electrolyte pair chemically inert at high temperatures. Thus, the solid state reaction between BSMF and CGO was performed for 50 h at 800 °C, 900 °C and 1000 °C in order to establish the reactivity. Fig. 7 depicts the after reaction XRD patterns for sample mixtures at a weight ration 1:1.

The XRD patterns of solid state mixture between BSMF and CGO for 50 h at 800 °C, 900 °C and 1000 °C, presented on Fig. 7, do not show any detectable additional phases. The three patterns are similar and testify to the good chemical compatibility of both materials after a long thermal treatment, and thus their possible association as cathode and electrolyte compounds.

## 4. Discussion

Two distinct behaviours have been demonstrated during the thermal analysis over the three studied perovskites. The first behaviour related to BSMF and BSCF samples demonstrated a final weight that was different than the initial weight. On the other side, for the GBC sample, no difference between initial and final weights was observed. The difference of crystalline structure with the ordered vacancy chains in the Brownmillerite structure [22] of GBC could explain this difference. Indeed, inside the BSMF and BSCF perovskite lattice, vacancies are randomly distributed leading to a tortuous pathway for the oxygen ion mobility. GBC brownmillerite structure presents the advantage of having well organized oxygen vacancies providing an easier removing and/or recovering of the oxygen molecules. This observation is of interest on the operating mode of a SOFC. Indeed, in the working configuration, the stack is submitted to frequent thermal cycling attributed to the start up and shut down of the system. The accumulation of weight loss during the successive heating and cooling steps may induce mechanical instability due to structural rearrangements and would be detrimental for the cathode layer. The structure of GBC is thus particularly interesting in this perspective.

Catalytic tests have demonstrated that LSM is not suitable as a cathode component for a single-chamber SOFC when the feed is hydrocarbon-based. This material is notably used for methane combustion [23,24] where both the Mn cation and the specific surface area are involved in the catalytic process. To our knowledge, few catalytic studies are reported over GBC, BSMF and BSCF. Shao et al. demonstrated the low activity of BSCF for propane conversion under stoichiometric conditions with an oxygen concentration of 20% at 600 °C [9]. Their observations are consistent with our results where BSCF is found poorly active until 600 °C compared with La-

based materials [25]. Unfortunately, their study was conducted under different $HC/O_2$ ratio which makes their data uncomparable. Elsewhere, a previous study on Ba-based perovskite pointed out the influence of dopants on the B site [26]. An improved methane conversion was observed for Mn addition while the addition of Co had little effect. That result corroborates with the observed trend in this work. This behaviour is attributed to the upper availability of oxygen species in Mn-doped perovskite. The inactivity of GBC under a methane atmosphere is very promising. The specific surface areas are summarized in Table 1, and can explain the low activity of our three samples. Indeed, as expected for perovskite materials, the values are very low in comparison with the LSM sample tested. The catalytic performances are in agreement with their thermodynamic properties where propane is more easily converted than methane based on the molecule stability. The addition of water and carbon dioxide to the methane/oxygen feed decreases the conversion is likely due to competitive adsorption for or both of these reagents with methane over the catalyst surface [27]. In addition, catalyst blockage by carbonate species due to the reaction between $CO_2$ and Ba cation [13] would reduce methane reactivity. From the aspect of their catalytic activity, BSCF and GBC are suitable under a SC-SOFC feed constituted by methane, water and carbon dioxide over the tested temperature range. The BSMF material is more active at higher temperatures with maximum catalytic activity at 550 °C, under our test conditions.

The evolution of ASR, here studied for the cathode materials over a CGO electrolyte in a symmetrical cell arrangement, is of primary interest. It clearly points out important discrepancies according to the electrode materials. The particular high values of ASR for BSMF compared with BSCF and GBC is attributed to a lower oxygen ionic conductivity inside the lattice contrary to GBC and BSCF known for their ability to reduce oxygen [7–10]. This gap can be assigned to the reducibility of the cation at the B site in the perovskite structure. Indeed, the Co cation in the +4 state is known to be unstable and easily reduced to the +3 state, leading to an improvement of the oxygen ionic conductivity by electrical neutrality. The opposite is observed for a Mn-containing perovskite where this cation is hardly reduced under air [8].

Regarding the numerous materials studied as electrolyte and cathode components, studies have been devoted to the reactivity of materials, notably GBC and BSCF. Powder reactivity for both of these materials with gadolinium doped-ceria had already been studied at high temperatures. The weak reactivity of GBC with the CGO electrolyte below 1000 °C is interesting. But at higher temperatures, it has been observed that the decomposition of the perovskite structure is due to the incorporation of Gd from the perovskite inside the CGO fluorite lattice [7]. The BSCF material has been shown to have a good chemical compatibility with CGO [21]. However, it is well known that between 900 °C and 1000 °C ceria and its eventual dopants are disposed due to the same cubic structure to migrate inside the BSCF lattice in the A or B site according to their ionic radii [12]. Herein, BSMF which can be compared to BSCF by the substitution of Co cation by Mn in the B-site, presents a particular high stability towards reactivity with CGO with no additional phase even after 50 h at 1000 °C under air atmosphere. A possible explanation is the difference of crystalline configuration between both materials. Indeed, contrary to BSCF, BSMF exhibits a hexagonal structure most probably hindering cation interdiffusion. In more, the difference in ionic radii of A sites ($Ba^{2+}$ = 1.35 Å and $Sr^{2+}$ = 1.58 Å), B sites ($Mn^{3+/4+}$ = 0.72/0.67 Å and $Fe^{2+/3+/4+}$ = 0.92/0.78/0.72 Å) and doped-ceria ($Gd^{3+}$ = 0.94 Å, $Ce^{4+}$ = 0.87 Å) seems critical to keep a crystalline structure intact after diffusion. Only Ce cation in the +3 state ($Ce^{3+}$ = 1.02 Å) would allow the formation of a new phase by diffusion in the A-site which is visibly not the case even after 50 h at 1000 °C under air.

## 5. Conclusions

Three perovskite materials have been investigated as possible cathode candidates for a single-chamber configuration SOFC in the intermediate temperature range. Characterizations have revealed a high thermal stability whereas catalytic tests under realistic feed conditions have shown that the conventional cathode material LSM is not applicable to the single-chamber configuration due an extremely high hydrocarbon conversion. BSCF, BSMF and GBC exhibit interesting catalytic features in the intermediate temperature range with no to little hydrocarbon conversion notably in the presence of water and carbon dioxide. Contrary to BSCF and GBC, study of powder reactivity for BSMF has shown it has excellent chemical compatibility with gadolinium doped-ceria, the most promising electrolyte material at temperatures around 600 °C. Nevertheless, ASRs measurements have shown important differences of polarization resistance and quite high values particularly for BSMF. All of these results confirm that the three tested materials would be suitable in the single-chamber configuration at intermediate temperatures but clearly point out that an optimization of the added dopants is required for a potential cathode in order to build a cell reaching the highest yields.

## Acknowledgements

Authors thank ADEME (Agence de l'Environnement de la Maîtrise de l'Energie) and Région de Bourgogne for the financial support. Scientific services of IRCELYON are fully acknowledged. Rhodia is also acknowledged for providing the ceria supports. The authors warmly acknowledge Dr Billy-Paul Holbrook for the English language improvement.

## References

[1] I. Riess, J. Power Sources 175 (1) (2008) 325–337.
[2] T. Suzuki, P. Jasinski, H.U. Anderson, F. Dogan, Electrochem. Solid-State Lett. 7 (11) (2004) A391–A393.
[3] M. Yano, A. Tomita, M. Sano, T. Hibino, Solid State Ionics 177 (39–40) (2007) 3351–3359.
[4] Z. Shao, J. Mederos, W.C. Chueh, S.M. Haile, J. Power Sources 162 (1) (2006) 589–596.
[5] T. Hibino, A. Hashimoto, T. Inoue, J.-i. Tokuno, S.-i. Yoshida, M. Sano, J. Electrochem. Soc. 147 (8) (2000) 2888–2892.
[6] N. Sakai, H. Kishimoto, K. Yamaji, T. Horita, M.E. Brito, H. Yokokawa, J. Electrochem. Soc. 154 (12) (2007) B1331–B1337.
[7] A. Tarancón, J. Peña-Martínez, D. Marrero-López, A. Morata, J.C. Ruiz-Morales, P. Núñez, Solid State Ionics 179 (40) (2008) 2372–2378.
[8] Y. Wu, T. Yu, B.-s. Dou, C.-x. Wang, X.-f. Xie, Z.-l. Yu, S.-r. Fan, Z.-r. Fan, L.-c. Wang, J. Catal. 120 (1) (1989) 88–107.
[9] Z. Shao, S.M. Haile, Nature 431 (7005) (2004) 170–173.
[10] B. Wei, Z. Lu, S.Y. Li, Y.Q. Liu, K.Y. Liu, W.H. Su, Electrochem. Solid State Lett. 8 (8) (2005) A428–A431.
[11] S. Li, Z. Lü, B. Wei, X. Huang, J. Miao, G. Cao, R. Zhu, W. Su, J. Alloys Compd. 426 (1–2) (2006) 408–414.
[12] K. Wang, R. Ran, W. Zhou, H. Gu, Z. Shao, J. Ahn, J. Power Sources 179 (1) (2008) 60–68.
[13] E. Bucher, A. Egger, G.B. Caraman, W. Sitte, J. Electrochem. Soc. 155 (11) (2008) B1218–B1224.
[14] A. Tarancón, D. Marrero-López, J. Peña-Martínez, J.C. Ruiz-Morales, P. Núñez, Solid State Ionics 179 (17–18) (2008) 611–618.
[15] Z. Shao, W. Yang, Y. Cong, H. Dong, J. Tong, G. Xiong, J. Membr. Sci. 172 (1–2) (2000) 177–188.
[16] G. Morra, A. Desmartin-Chomel, C. Daniel, U. Ravon, D. Farrusseng, R. Cowan, M. Krusche, C. Mirodatos, Chem. Eng. J. 138 (1–3) (2008) 379–388.
[17] B.C.H. Steele, A. Heinzel, Nature 414 (6861) (2001) 345–352.
[18] C. Frontera, J.L. García-Muñoz, A. Llobet, L. Mañosa, M.A.G. Aranda, J. Solid State Chem. 171 (1–2) (2003) 349–352.
[19] A.K. Demin, F.Y. Gulbis, Solid State Ionics 135 (1–4) (2000) 451–456.
[20] E. Perry Murray, S.A. Barnett, Solid State Ionics 143 (3–4) (2001) 265–273.
[21] Z. Duan, M. Yang, A. Yan, Z. Hou, Y. Dong, Y. Chong, M. Cheng, W. Yang, J. Power Sources 160 (1) (2006) 57–64.
[22] G.B. Zhang, D.M. Smyth, Solid State Ionics 82 (3–4) (1995) 161–172.

[23] S. Ponce, M.A. Peña, J.L.G. Fierro, Appl. Catal. B: Environ. 24 (3–4) (2000) 193–205.
[24] L. Marchetti, L. Forni, Appl. Catal. B: Environ. 15 (3–4) (1998) 179–187.
[25] T. Suzuki, P. Jasinski, H.U. Anderson, F. Dogan, J. Electrochem. Soc. 151 (10) (2004) A1678–A1682.
[26] N. Gunasekaran, S. Rajadurai, J.J. Carberry, N. Bakshi, C.B. Alcock, Solid State Ionics 73 (3–4) (1994) 289–295.
[27] C.-H. Wang, C.-L. Chen, H.-S. Weng, Chemosphere 57 (9) (2004) 1131–1138.